JOURNAL OF MODERN OPTICS, 2017
VOL. 64, NOS. 10–11, 1042–1053
https://doi.org/10.1080/09500340.2016.1278282

Taylor & Francis
Taylor & Francis Group

Simultaneous observation of transient and final state dynamics in ultrafast strong-field excitation via time-resolved photoelectron spectroscopy

Hendrike Braun[a], Tim Bayer[b], Dominik Pengel[b], Matthias Wollenhaupt[b] and Thomas Baumert[a]

[a]Institut für Physik, Universität Kassel, Kassel, Germany; [b]Institut für Physik, Carl von Ossietzky Universität Oldenburg, Oldenburg, Germany

ABSTRACT

Strong-field coherent control deals with the efficient excitation of a quantum system into a preselected final state. In order to understand the underlying control mechanisms, the transient dynamics of the laser-dressed states need to be considered in addition. In this paper, we present a route towards a complete picture of non-perturbative coherent control. To this end, we study near-resonant chirped excitation of potassium atoms as a model system for resonant strong-field control. Combining a two-colour pump–probe scheme with photoelectron spectroscopy, we simultaneously observe final state and transient excitation dynamics in the strongly driven atom. As demonstrated on the prototype scenario, the scheme enables a detailed understanding of the physical mechanisms governing the interaction. Our results highlight the power of two-colour time-resolved photoelectron spectroscopy to shed light onto the different aspects of non-perturbative coherent control.

ARTICLE HISTORY
Received 20 October 2016
Accepted 21 December 2016

KEYWORDS
Femtosecond laser pulses; ultrafast pulse shaping; two-colour time-resolved photoelectron spectroscopy; strong-field coherent control; rapid adiabatic passage; selective population of dressed states

1. Introduction

Traditionally, coherent control is interested in the selective excitation of a quantum system into a desired final state after the interaction with a suitably shaped ultrashort laser field (*1*–*3*). The actual control takes place during the coherent interaction. Strong-field interactions, associated with efficient population transfer, lead to a significant distortion of the system's energy landscape due to the dynamic Stark effect. This makes an analysis of the physical control mechanism only on the basis of the bare system states, i.e. the eigenstates of the unperturbed system, difficult. In strong-field control, the transient dynamics of the laser-dressed states, i.e. the eigenstates of the interacting system, need to be considered in addition. Recently, we demonstrated efficient final state control in molecules by controlling the dressed state dynamics of the system (*4*, *5*), where the design of the control fields was based on a detailed knowledge of the physical mechanism. These experiments underscore the importance to analyse both the transient dynamics and the resulting final state populations in order to obtain a comprehensive picture of strong-field coherent control. Here, we present experimental studies on strong-field control exerted via intense chirped femtosecond laser pulses. Chirped pulses are used as a prototype for shaped pulses with controllable envelope and time-varying detuning. The quantum system under study is the potassium atom which serves as a model system for resonant strong-field control. In the experiments, we employ a two-colour pump–probe scheme for time-resolved measurements. The optical scheme is combined with photoelectron spectroscopy being a sensitive probe of both the populations and the quantum phase of the coherently excited system. By this means, we are able to simultaneously observe transient and final state dynamics of the atom interacting non-perturbatively with the shaped laser pulses.

For resonant interaction, chirped excitation is closely connected to rapid adiabatic passage (RAP) (*6*) being one of the most well-established schemes for efficient strong-field control. Population inversion via RAP has been demonstrated on atomic and molecular two-state and multi-state systems (*6*–*14*).

RAP is characterized by highly efficient and robust population transfer. The physical mechanism is based on adiabatic interaction between the guiding laser field and the driven system. The basic requirements are strong couplings and sufficiently slow field variations in terms of envelope and detuning. Under adiabatic conditions, the total system remains in an eigenstate, i.e. in a dressed state preselected by the initial detuning, throughout the entire interaction. In this manner, RAP transiently realizes the selective population of dressed states (SPODS) (*15*, *16*).

In this contribution, we present a detailed investigation of both the transient and the final state dynamics induced by intense resonant chirped laser pulses.

CONTACT Hendrike Braun braun@physik.uni-kassel.de

Specifically, we observe population inversion and creation of superposition states by chirped excitation, transient dressing of the system and selective population of a single dressed state. In addition, we investigate the onset of adiabaticity and deviation thereof to explore further routes to coherent control in multi-state systems.

The paper is structured as follows. We start in Section 2 by introducing the excitation scheme of potassium atoms exposed to a sequence of an intense resonant control pulse and a time-delayed non-resonant probe pulse. In Section 3, we describe the experimental implementation of the two-colour scheme based on time-resolved photoelectron spectroscopy. Our experimental results are presented in Section 4. The experiments were divided into four separate studies covering different strong-field excitation scenarios. Initially, we employed the two-colour set-up to map Rabi oscillations in the resonantly driven atom (Section 4.1) in order to calibrate the interaction strength and identify the non-perturbative excitation regime for the following experiments. Next, we performed time-resolved studies on non-perturbative chirped excitation to highlight different aspects of RAP (Section 4.2). In a series of two-colour pump–probe experiments, we simultaneously measured the transient and final state dynamics to obtain the full picture of the control exerted by the chirped pulse. The third experiment is dedicated to the chirp dependence of the excitation (Section 4.3). Probing the driven system either during or after the interaction with the chirped pulse allows us to examine the influence of the chirp on the transient dynamics and the final state of the atom, respectively. Section 5 ends the paper with a brief summary and conclusion. The appendix contains a study on photon locking via multi-pulse sequences as a complementary example based on impulsive excitation and discrete temporal phase jumps.

2. Excitation scheme

Figure 1(a) shows the excitation and ionization schemes for ground state (4*s*) potassium atoms interacting with an intense, $\lambda_0 = 790$ nm, $\Delta t = 30$ fs laser pulse (referred to as IR pump or control pulse) and a weak $\lambda_p = 570$ nm, $\Delta t_p = 20$ fs laser pulse (VIS probe pulse) which is time delayed by a variable delay τ. Under near-resonant non-perturbative excitation by the control pulse, the excited 4*p* state splits into two dressed states due to the resonant dynamic Stark effect. Simultaneous two-photon ionization maps these dressed states into the photoionization continuum, giving rise to the Autler–Townes (AT) doublet in the measured photoelectron spectrum (PES) centred around 0.4 eV (cf. Figure 1(b)). Excitation exactly on resonance at 768 nm using band width-limited (BWL) control pulses leads to a symmetric AT doublet, indicating equal population of both dressed states. Near-resonant red-detuned excitation, as in our experiments, leads to a preferential population of the lower dressed state and therefore to a slight asymmetry of the AT doublet in favour of the low energetic AT component. Time-delayed probing of the system by the VIS pulse, $\tau \gg \Delta t$, creates additional signals in the PES. Two-photon ionization from the 4*s* state creates photoelectrons near the threshold at about 0.05 eV, mapping the ground state population. The signal at 1.6 eV maps the population of the excited 4*p* state. If the VIS pulse probes the system during the interaction with the control pulse, i.e. $|\tau| < \Delta t$, the probe pulse too maps the dressed states rather than the bare states of the resonantly driven atom (cf. Figure 1(c) and (d)). In this case, the probe signals also exhibit the AT splitting. Moreover, two-photon ionization by frequency mixing of control and probe pulses, i.e. simultaneous absorption of photons from both pulses, creates photoelectrons with kinetic energies around 1.0 eV. Due to the required temporal overlap of pump and probe pulse, these electrons also map the dressed states, so that the exact energy of the signals is determined by the dynamic Stark shift.

For an accurate description of the final state dynamics observed in Section 4.2.2, the fine structure splitting of the 4*p* state into the $4p_{1/2}$ and the $4p_{3/2}$ states has to be taken into account. In the potassium atom, the energetic difference between the 4*p* fine structure components is only $E_{3/2} - E_{1/2} = 7$ m eV, as compared to the spectral bandwidth of the IR pulse of $\Delta\omega > 50$ m eV (see Figure 7 for an illustration of the potassium fine structure levels in relation to the laser spectral width). As a consequence, excitation by the control pulse in general leads to the formation of a bound electron wave packet (*17*, *18*) beating with a time period of $T_{beat} = {}^{2\pi\hbar}/_{(E_{3/2}-E_{1/2})} = 578$ fs (cf. Section 4.2.2). Another manifestation of the three-state character of the atom is the emergence of a third dressed state. It was shown that selective population of the third dressed state is achieved by discrete spectral phase modulation in between the two fine structure resonances (*19*, *20*). However, because in this contribution only continuous and slowly varying spectral phase modulation functions (quadratic and sinusoidal) are employed, the third dressed state plays no prominent role here.

3. Experimental set-up

The experimental two-colour pump–probe set-up is depicted schematically in Figure 2. Our amplified Ti:Sa laser system generates femtosecond laser pulses with a central wavelength of $\lambda_0 = 790$ nm, an intensity FWHM of $\Delta t = 30$ fs at a repetition rate of 1 kHz. After passing

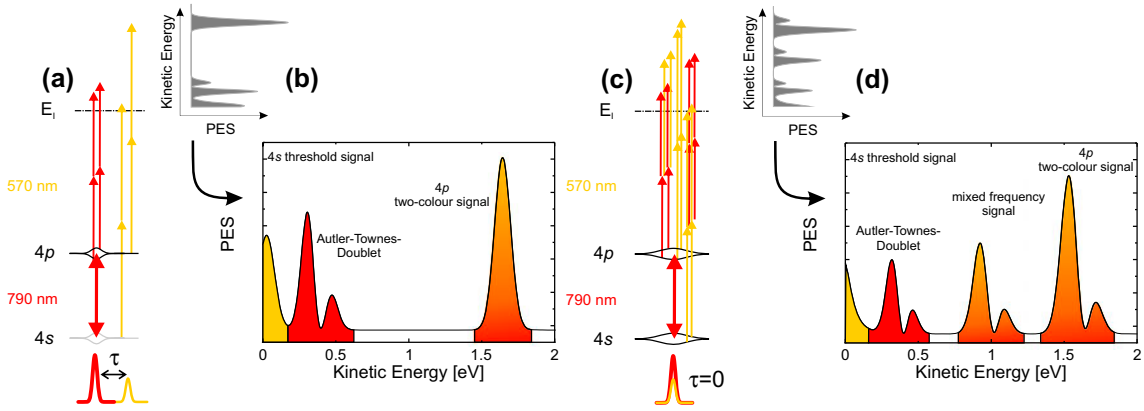

Figure 1. (a) and (c) Excitation and ionization schemes of potassium atoms interacting with a strong resonant IR femtosecond laser pulse (red arrows) and a weak non-resonant probe pulse (yellow arrows) time delayed by τ. (b) and (d) Simulated photoelectron spectra resulting from the laser–atom interaction as depicted in (a) and (c).

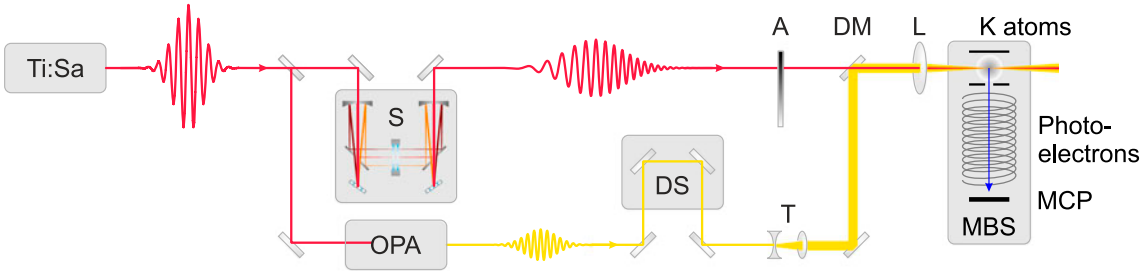

Figure 2. Experimental two-colour pump–probe set-up for time-resolved photoelectron spectroscopy. For a detailed description see main text.

a 50 : 50 beamsplitter, one part of the IR beam is used to pump an optical parametric amplifier (OPA) which provides VIS probe pulses with a central wavelength of $\lambda_p = 570\,\text{nm}$ and a duration of $\Delta t_p = 20\,\text{fs}$. The other part enters our homebuilt $4f$ pulse shaper based on a liquid crystal spatial light modulator (LC-SLM) (*21*, *22*) for spectral phase modulation. The shaped IR pulses are sent via a polarization rotating periscope and a variable ND attenuator (A) towards the experiment. The VIS probe pulses pass a variable delay stage (DS) to introduce the time delay τ and a magnifying telescope (T). The telescope serves to enhance the probe beam diameter to about three times the diameter of the control pulse for tight focussing. By this means, only the central part of the pump focus is probed to minimize the effect of volume averaging in the probe signals. Averaging over the intensity distribution of the pump beam, i.e. over different excitation volumes, leads to a blurring of non-robust strong-field effect such as Rabi cycling and photon locking (*14*, *19*). Pump and probe beams are combined by a dichroic mirror (DM) and focused collinearly by an $f = 300\,\text{mm}$ lens (L) into the interaction region of a magnetic bottle time-of-flight photoelectron spectrometer (MBS). Here, they interact with potassium atoms in the gas phase from an alkali metal dispenser source (SAES Getters). Photoelectrons released during the interaction are collected by the magnetic bottle and measured with kinetic energy resolution by an MCP detector in chevron configuration. Depending on the time delay τ between IR control and VIS probe pulses, different signals are observed in the measured PES (see Section 2). The time delay is continuously variable between $\tau = -1\,\text{ps}$ (probe before pump) up to $\tau = +3\,\text{ps}$ (probe after pump) in order to cover several periods T_{beat} of the fine structure beating (see Section 4.2.2) and to avoid unwanted overlap of the probe pulse with a strongly chirped control pulse for final state investigations (see Section 4.3.1).

4. Experimental results

In the experiments, we applied the two-colour pump–probe scheme to highlight different aspects of the strong-field interaction of shaped IR control pulses with the atomic system. As a starting point in Section 4.1, we measured Rabi cycling in the near-resonantly driven atom using BWL control pulses to gain an overview of the interaction strength and the onset of non-perturbative excitation. In Section 4.2, we present results of time-resolved measurements on RAP using chirped control pulses but keeping the chirp parameter fixed. The chirp dependence of the excitation process is addressed subsequently in Section 4.3.

4.1. Rabi oscillations

The measurement of Rabi oscillations as a function of the control pulse energy serves to separate the perturbative weak-field regime, characterized by little to no population transfer, from the non-perturbative regime relevant to the following experiments on chirped excitation. In order to identify the onset of the non-perturbative regime, we measured the final populations of the atomic ground state 4*s* and resonantly excited state 4*p* by probing the atom after the interaction with a BWL control pulse for various control pulse energies. The experimental results are shown in Figure 3. The two-colour photoelectron signals at 0.05 and 1.6 eV reveal an anti-correlated oscillatory behaviour of the 4*s* and 4*p* population attributed to Rabi cycling in the near-resonantly driven atom. A complete population transfer is suppressed by the red-detuning of the control pulse. Therefore, the observed Rabi oscillation is not fully modulated. The double-peak contribution, which appears around 0.4 eV with increasing pulse energy, is the AT doublet from direct photoionization by the control pulse. As discussed in Section 2, the slight asymmetry of the doublet in favour of the low energetic component is due to the red-detuned excitation which promotes the lower dressed state during the interaction. Figure 4 shows simulations based on the numerical solution of the time-dependent Schrödinger equation for a three-level atom interacting with the intense IR control pulse and perturbative two-photon photoionization by the control probe pulse sequence (*20*, *21*, *23*). In order to match the experimental conditions, we accounted for residual intensity averaging over the central region of the IR laser focus, assuming a Gaussian IR laser beam profile (*5*). The simulation results are in good agreement with the measured data. Simulations performed under idealized conditions, i.e. for a single laser peak intensity, yield a 50% larger Rabi oscillation frequency. Thus, in a non-robust strong-field scenario, such as Rabi cycling, focal regions of lower intensity need to be included in the calculations for an adequate modelling of the experimental results.

From the results in Figure 3 we infer that for control pulse energies larger than 0.1 μJ, i.e. a population transfer of more than 50%, the interaction is definitely non-perturbative. Therefore, to ensure strong-field interaction conditions in the control experiments presented in the following sections, we chose pulse energies around 0.9 μJ. Via the ponderomotive shift in the ionization of xenon atoms, we determined this pulse energy to correspond to a peak intensity of the BWL pulse of $I_0 \approx 5 \times 10^{11}\,\mathrm{W/cm^2}$.

4.2. Time-resolved studies

In this section, we present time-resolved studies on non-perturbative resonant chirped excitation of the atomic system. The first experiment (Section 4.2.1) focuses on the transient, i.e., dressed state dynamics of the driven atom by overlapping probe and control pulses in time. In the second experiment (Section 4.2.2), an extended delay range is scanned to monitor the dynamics of fine structure wave packets excited by chirped control pulses of different chirp parameters.

4.2.1. Observation of transient dynamics

Probing the atom at different times during the interaction with an intense shaped control pulse provides rich information on the transient time evolution of the system, typically in terms of the dressed states, all the way to the final system state at the end of the control pulse. Figure 5(b) shows PES measured as a function of the time delay between the probe and a down-chirped control pulse varied between $\tau = -655$ fs (probe before pump) and $\tau = +680$ fs (probe after pump). The negative chirp was introduced by the quadratic phase mask $\varphi(\omega) = \phi_2 \cdot (\omega - \omega_0)^2$ with $\phi_2 = -2000\,\mathrm{fs}^2$ and $\omega_0 = 2\pi c/\lambda_0$ applied to the LC-SLM. The chirp results in a temporal stretching of the control pulse to a duration of $\Delta t_{chirp} = 370$ fs (*24*). To ensure non-perturbative interaction conditions (see Section 4.1), the energy of the control pulse was set to 0.8 μJ. The different signals observed in the PES provide insight into different aspects of the laser-induced dynamics. Figure 5(c) shows selected spectra from the delay scan in (b) for the negative delay $\tau = -580$ fs (blue; beginning of interaction), $\tau = 0$ fs (black; during the interaction) and the positive delay $\tau = +650$ fs (red; end of interaction).

At the beginning of the interaction, $\tau < \Delta t_{chirp}$, the atom is in the ground state as indicated by the dominant 4*s* signal in the blue PES. The minor contribution from the 4*p* state is due to the finite overlap of probe and control pulses at small negative delays. With the onset of the chirped control pulse, the population is successively transferred to the 4*p* state. This is seen by the monotonous rise of the 4*p* signal around $\tau = 0$ fs (cf. black PES). After the interaction, the system is excited to the 4*p* state as indicated by the depletion of the 4*s* ground state signal in the PES. Efficient continuous, i.e., non-oscillatory excitation of the system by the intense chirped control pulse is a clear signature of RAP in view of the bare atomic states.

Regarding the dressed state dynamics, mapped into the AT doublet observed around 0.4 eV, further interesting details of the interaction are revealed. The strong asymmetry of the AT doublet and, in particular, the absence of the low-energetic AT component (cf. Figure 3 (b)) hint towards the selective population of the upper dressed state by the down-chirped control pulse. This observation is in accordance with an adiabatic passage scenario induced by a negative chirp. In this case, the

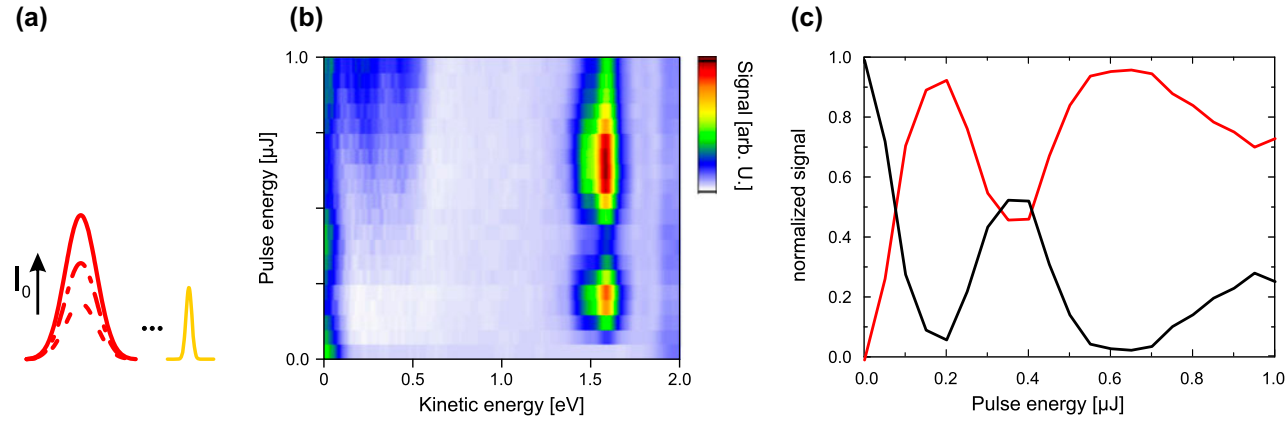

Figure 3. (a) The delay between pump and probe pulse is fixed at $\tau = 1\,\mathrm{ps}$. The intensity of the pump pulse is varied via the pulse energy. (b) Measured PES resulting from a variation of the pulse intensity. The signals created by the time-delayed probe pulse from the potassium 4*s* state (at 0.05 eV) and 4*p* multiplet (at 1.6 eV) oscillate anti-correlated with increasing pulse energy, indicating Rabi oscillations in the near-resonantly driven atom. (c) Integrated signals from the 4*s* state (black) and the 4*p* state (red). The sum of the signals has been normalized to 1.

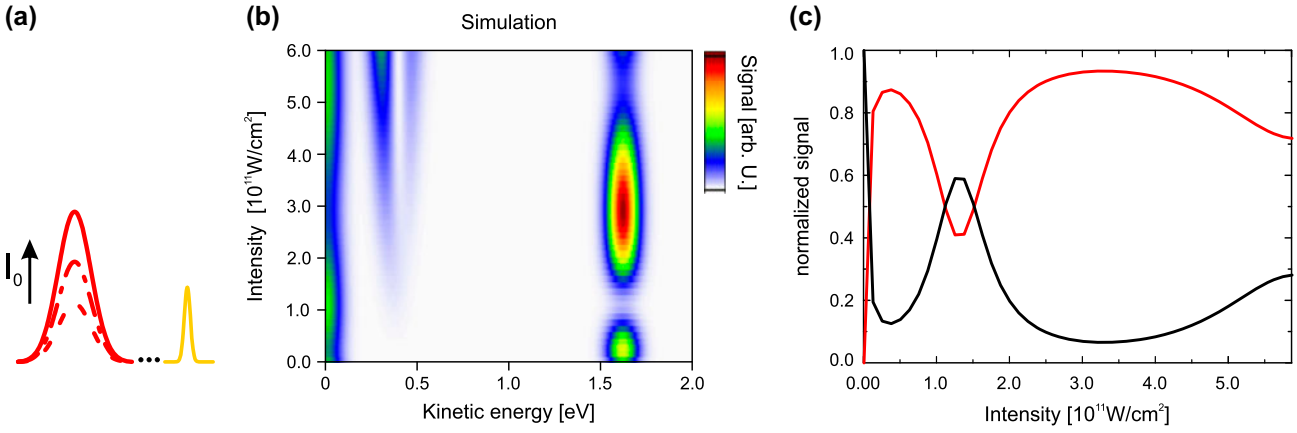

Figure 4. (a) The delay between control and probe pulses is fixed at $\tau = 1\,\mathrm{ps}$. The intensity of the control pulse is varied. (b) Simulated PES for potassium atoms interacting with IR control pulses of increasing intensity and time-delayed probe pulses. (c) Integrated and normalized signals from the 4*s* state (black) and the 4*p* state (red). The average over the focal intensity distribution of the control pulse was taken into account.

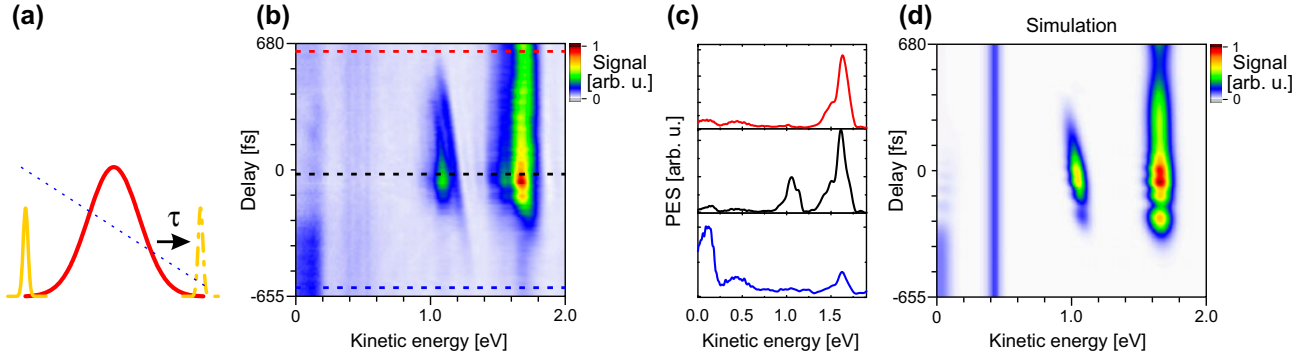

Figure 5. (a) The time delay τ between a chirped IR control pulse and the VIS probe pulse is varied around $\tau = 0\,\mathrm{fs}$ (temporal overlap region). The dashed blue line illustrates the decreasing instantaneous frequency $\omega_{inst}(t)$ of the chirped IR control pulse. (b) Measured PES resulting from a delay scan of the probe pulse across the chirped control pulse. (c) Selected spectra marked by dashed lines in (b). The spectra are scaled individually. (d) Simulation results.

system is steered adiabatically along the upper dressed state throughout the entire interaction (*6*, *15*). Since the AT signal is created directly by the control pulse, it is independent of the time delay. The reduced signal strength in comparison to the PES shown in Figure 3(b) is explained by the reduction of peak intensity of the chirped pulse in comparison to the BWL pulse.

In the overlap region of pump and probe pulse, not only the AT signal generated by the IR pulse reflects the dressed state energy splitting. Also the signals from the 4*s* ground state and the 4*p* state created by the probe pulse during the interaction with the control pulse map the dressed states and, therefore, exhibit the AT splitting. Due to the selective population of the upper dressed state, the 4*s* signal shifts towards higher energies around $\tau = 0$ fs (see also the simulation result in Figure 5(d)). This demonstrates the power of the two-colour scheme to extract the dressed state dynamics from both the excited state and the ground state signals.

The mixing signal centred at 1.0 eV and observed in the temporal overlap region of control and probe pulses (cf. black spectrum in Figure 5(b)) also maps the dressed states. In addition to the dynamic Stark shift, the energy of these photoelectrons is modulated by the instantaneous frequency of the chirped control pulse which contributes one photon to the ionization process. Therefore, due to the negative linear chirp, the mixing signal shifts linearly towards smaller energies for increasing τ.

Again, the simulation results shown in Figure 5(d) are in convincing agreement with the experiment. The modulation of the 4*p* signal observed for large delay times when the control pulse has already decayed, $\tau \gg \Delta t_{chirp}$, is due to the creation of a coherent superposition of the two fine structure components $4p_{1/2}$ and $4p_{3/2}$. Girard et al. consequently attributed these oscillations to the creation of a spin orbit wave packet (*17*, *18*, *25*–*27*). Closer investigation of the dynamics of this bound electron wave packet and its control is the subject of the next section.

4.2.2. Control of fine structure wave packet dynamics

The essence of RAP in a two-state system is robust bare state inversion achieved by steering the system adiabatically along a preselected dressed state (also termed adiabatic states in this context). In multi-state systems, where more than one final state is available for selective excitation, deliberately breaking the adiabaticity adds another degree of freedom to the applicable control (*20*). Semi-adiabatic scenarios allow for transitions between dressed states to navigate the system into a desired final state or superposition of states. Parameters which influence the adiabaticity of the laser-induced excitation are, e.g., the laser peak intensity, the detuning from resonance and, in particular, the chirp. As a prototype example of semi-adiabatic control, we investigated the formation and evolution of the electronic fine structure wave packet by chirped near-resonant excitation of the potassium atom. The chirp parameter ϕ_2 is used to control the population distribution among the two fine structure components and, thus, to manipulate the dynamics of the excited electron wave packet. Figure 6 shows measured two-colour PES from a long-range delay scan between $\tau = -970$ fs and $\tau = 2370$ fs, i.e. over several periods T_{beat} of the fine structure beating (see Section 2). In Figure 6(a), the atomic system is excited by a BWL control pulse with a pulse energy of 0.9μJ. After the interaction with the control pulse, the 4*p* signal exhibits a slow oscillation which reflects the time evolution of the excited fine structure wave packet. The integrated 4*p* signal as a function of τ is plotted in Figure 6(d) (blue squares). A sinusoidal fit of the beating pattern (blue line) yields a time constant of $T_{fit} = 579$ fs, in excellent agreement with the theoretical value of T_{beat}. In contrast, Figure 6(b) shows the same parameter variation for the down-chirped control pulse discussed in Section 4.2.1. This measurement is an extension of the measurement presented in Figure 5 towards longer delay times. The integrated 4*p* signal is plotted as light green squares in Figure 6(d). In comparison to the BWL excitation in (a), the amplitude of the oscillation in the 4*p* signal is reduced, indicating the excitation of a pure state rather than a wave packet. Adiabatic passage induced by a down-chirped control pulse suggests the selective excitation of the energetically higher lying fine structure component (*9*, *28*). This is supported by the simulation results shown in Figure 7(a)–(c), where a negatively chirped pulse steers the three-level atom selectively into the $4p_{3/2}$ state – despite the red-detuning of the control pulse. By inversion of the chirp, we obtained the experimental results presented in Figure 6(c) and plotted as dark green squares in d). Compared to the down-chirped case, the amplitude of the fine structure beating is strongly enhanced (factor 5.4), indicating the efficient creation of a superposition state by the up-chirped pulse. This finding is confirmed by the simulation results in Figure 7(d)–(f), where the up-chirped control pulse excites an efficient superposition of states $4p_{1/2}$ (60%) and $4p_{3/2}$ (40%). In addition, the reduction of the 4*s* signal in Figure 6(c) as compared to the BWL excitation in (a) indicates a more efficient population transfer to the 4*p* doublet by the chirped pulse.

The reason for the observed asymmetry of the final state with respect to the chirp sign lies in the red-detuned excitation. Fully resonant simulations reveal a symmetric behaviour of the final state population with respect to the chirp sign. For sufficiently large positive chirp, the $4p_{1/2}$ state is populated selectively via RAP, whereas in-

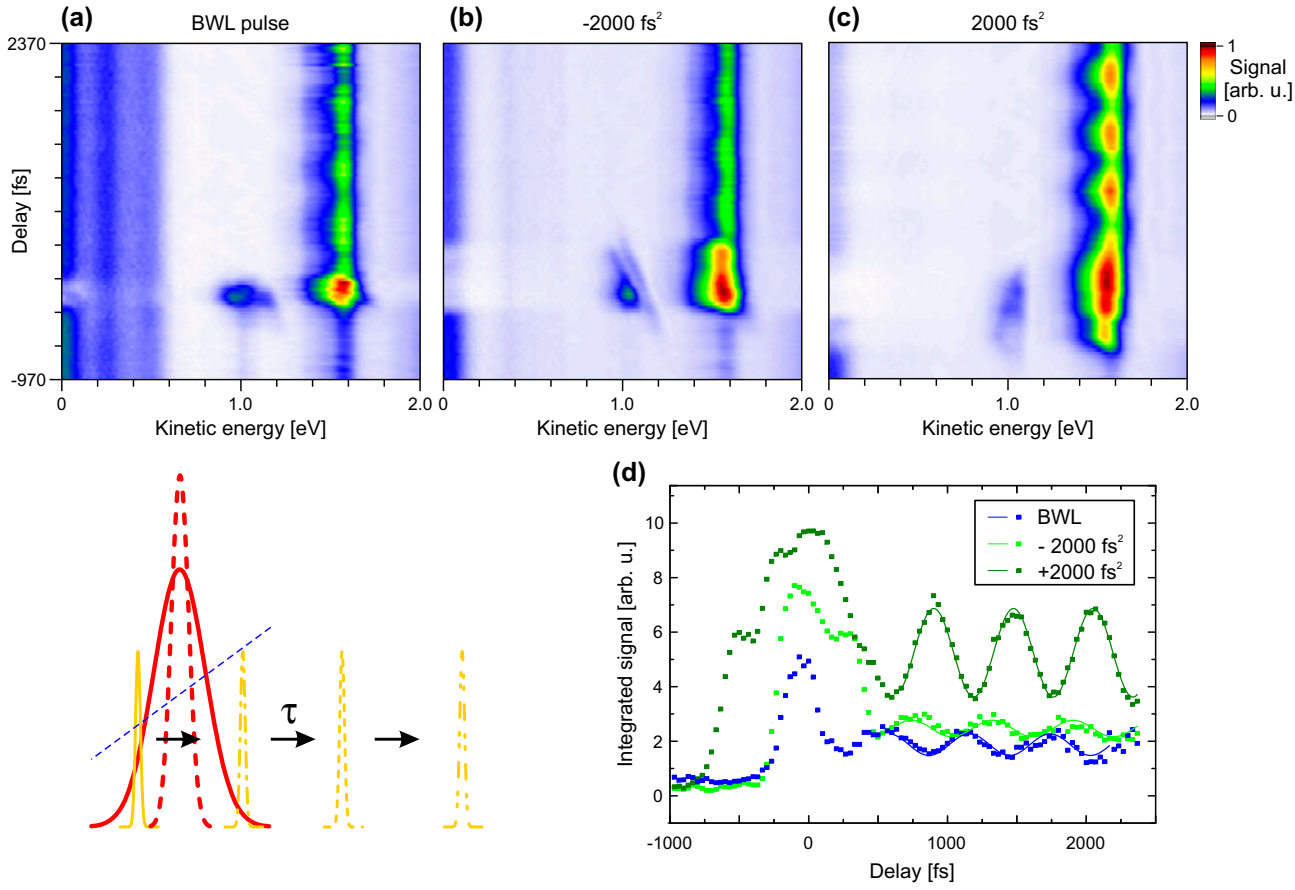

Figure 6. (a)–(c) Measured PES from pump–probe scans using differently chirped control pulses. The dashed blue line in the pictogram represents the increasing instantaneous frequency $\omega_{inst}(t)$ of a positively chirped control pulse. (a) BWL control pulse: creation of a fine structure wave packet, as can be seen from the periodically modulated signal from the 4*p* doublet. The oscillation frequency of $T_{beat} = 579$ fs reflects the energy separation of the two fine structure components. (b) Negatively chirped control pulse: the reduction of the modulation depth reveals the selective population of the upper fine structure component via RAP. (c) Positively chirped control pulse: A coherent superposition of the two fine structure components is efficiently excited, visible in the increased signal of the 4*p* doublet and the deep modulation thereof. (d) Integrated 4*p* signals from the pump–probe scans (squares) and sinusoidal fits (solid lines).

version of the chirp sign switches the population transfer selectively to the $4p_{3/2}$ state. Figure 7 shows simulation results for the two experimental scenarios shown in Figure 6(b) and (c). In the case of the down-chirped laser pulse (left column), the instantaneous laser frequency sweeps across the system resonance at an early time during the interaction. Almost no population is transferred between the dressed states at the corresponding avoided crossing marked by the green circle. As a result, the entire population is transferred adiabatically into the upper fine structure component $4p_{3/2}$. Since the system is excited into an eigenstate, no final state dynamics is observed in Figure 6(b). For the up-chirped laser pulse (right column), the resonance is crossed at a later time when the laser pulse is already decaying (red circle). As seen in the inset to Figure 7(f), a part of the population of the initially populated lower dressed state escapes to the intermediate dressed state. In this case, the atom is steered into a coherent superposition of the two fine structure components $4p_{1/2}$ and $4p_{3/2}$ by the end of the control pulse. The ensuing wave packet dynamics are expressed in the pronounced 4*p* beating observed in Figure 6(c). A quantitative adiabaticity analysis of chirped excitation of potassium atoms based on (*8*) can be found in (*15*).

4.3. Chirp-dependent excitation

The time-resolved two-colour measurements presented in Figures 5 and 6 unveil the rich dynamics in the atomic system during and after the interaction with the chirped control pulses. In order to further deepen the understanding of the interaction and, in particular, to investigate the transition from the impulsive non-adiabatic to the robust adiabatic excitation regime, we performed additional chirp-dependent studies at fixed delay times. As special times of interest, we examined a sufficiently large delay of $\tau = 1$ ps (Section 4.3.1) to detect the final state of the atom after the interaction with the chirped control

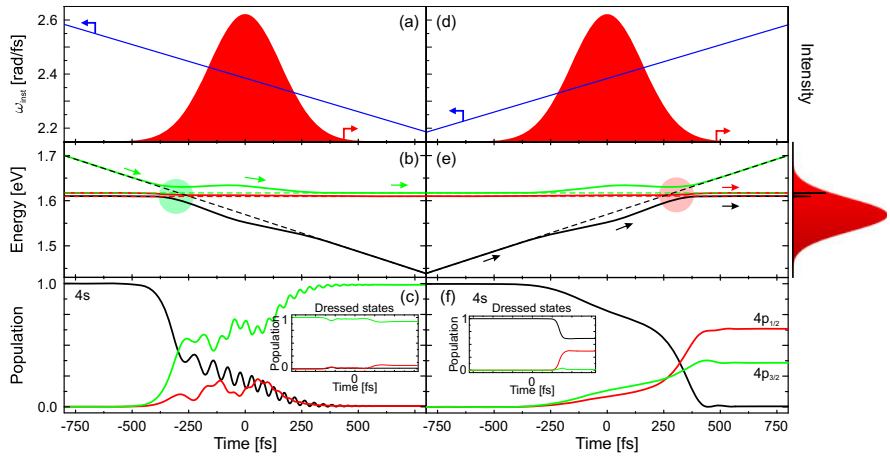

Figure 7. Simulated dynamics of a potassium atom for the interaction with a negatively (left column) and a positively (right column) chirped IR control pulse. (a) and (d) illustrate the intensity profiles (red) and the instantaneous frequencies (blue) of the chirped pulses. The energies of the dressed states (solid lines) and the bare states (dashed lines) are depicted in (b) and (e). The green and red circles indicate the avoided crossings of the dressed states where the chirp crosses the bare state resonance. The arrows indicate the flow of the dressed state populations. In (c) and (f), the bare state population dynamics are shown, along with the dressed state dynamics (insets). The energetic positions of the fine structure resonances relative to the control pulse spectrum are indicated on the right.

pulse, and the temporal overlap of both pulses at $\tau = 0$ fs (Section 4.3.2) to capture the transient interaction dynamics.

4.3.1. Influence on the final state

First, we investigate the chirp dependence of the final system state by fixing the time delay to $\tau = 1$ ps. For a variation of the chirp parameter ϕ_2 between –2000 fs^2 and 2000 fs^2, this delay is much larger than the duration Δt_{chirp} of the chirped control pulses ($\Delta t_{chirp} = 370$ fs for $|\phi_2| = 2000$ fs^2). The pulse energy was set to 1,1μJ to ensure non-perturbative excitation conditions. The experimental results are displayed in Figure 8(b), supported by the simulation results in (c). For BWL excitation, $\phi_2 = 0$, a small $4p$ signal is observed, as expected from the Rabi oscillations in Figure 3(c). For increasing values of $|\phi_2|$, the $4p$ population rises monotonously at the expense of the $4s$ population. For negative chirp, the $4p$ population starts to saturate at about $\phi_2 = -1000$ fs^2 indicating the complete inversion of the atom. This marks the onset of the adiabatic excitation regime associated with RAP. As discussed in Section 4.2.2, the red-detuned excitation promotes adiabaticity for negative chirps, while hampering adiabatic interaction for positive chirps. Therefore, for increasing positive values of ϕ_2, the behaviour of the $4p$ signal is not strictly monotonic. Inversion of the atom is achieved at about $\phi_2 = +1500$ fs^2. For even larger values of ϕ_2, the $4p$ signal decreases again due to the induced fine structure wave packet dynamics (cf. Figure 6(c)). Because the chirp of the control pulse determines the initial conditions of the fine structure beating, as clearly seen in Figure 6(d), the coherence of the $4p$ doublet is probed at different phases, leading to a modulation of the ionization probability (*17*).

The AT doublet at 0.4 eV reveals the transient dressed state dynamics. At $\phi_2 = 0$, we again observe the slight asymmetry due to red-detuned excitation by the BWL pulse (cf. Sections 2 and 4.1). For increasing positive values of ϕ_2, the high-energetic AT component vanishes completely from the PES, indicating the selective population of the lower dressed state during the most intense part of the up-chirped control pulse (*15*). Vice versa, for negative values of ϕ_2, i.e. down-chirped control pulses, the upper dressed state is populated selectively. The realization of SPODS via resonant chirped excitation is the transient signature of RAP. In both cases, the dressed state energy splitting shrinks due to the lowered peak intensity of the chirped pulses for fixed pulse energy. The decrease in peak intensity also strongly affects the non-linear ionization efficiency leading to the observed reduction of overall AT signal yield. Nevertheless, the direct ionization by the control pulse provides a sensitive probe of the transient system dynamics.

4.3.2. Influence on transient dynamics

For $\tau = 0$ fs, the system is probed during the non-perturbative resonant interaction with the control pulse. Therefore, all photoelectron signals including those generated by the probe pulse map the population and energies of dressed states. PES measured by scanning the chirp of the control pulse at $\tau = 0$ fs are presented in Figure 9(b) and (c). All signals show a behaviour similar to the AT doublet observed in Figure 8. For excitation with the BWL pump pulse ($\phi_2 = 0$), the energy splitting of the dressed states in the strongly driven system results in a

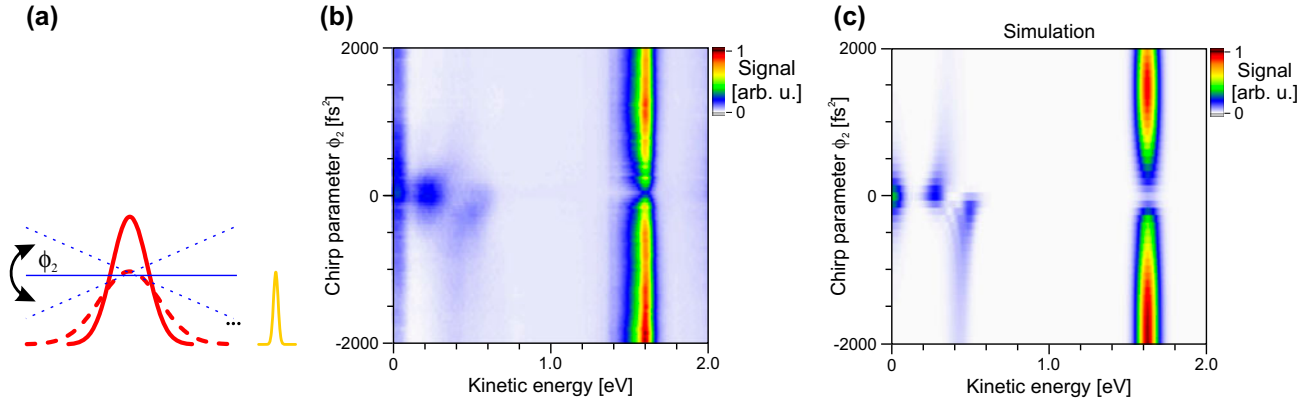

Figure 8. (a) The chirp of the IR control pulse is varied while the time delay τ between control and probe pulses is fixed. The blue lines illustrate the instantaneous frequencies $\omega_{inst}(t)$ of the different chirped control pulses. (b) Measured PES resulting from a chirp scan of the control pulse and a probing at a fixed time delay after the interaction. For large chirp parameters, the ground state population is efficiently transferred to the 4*p* state, as indicated by the 4*p* signal. The signal of the AT doublet reveals the dynamics of the dressed states during the excitation with the chirped control pulses. (c) Simulated PES are in excellent agreement with the measurements.

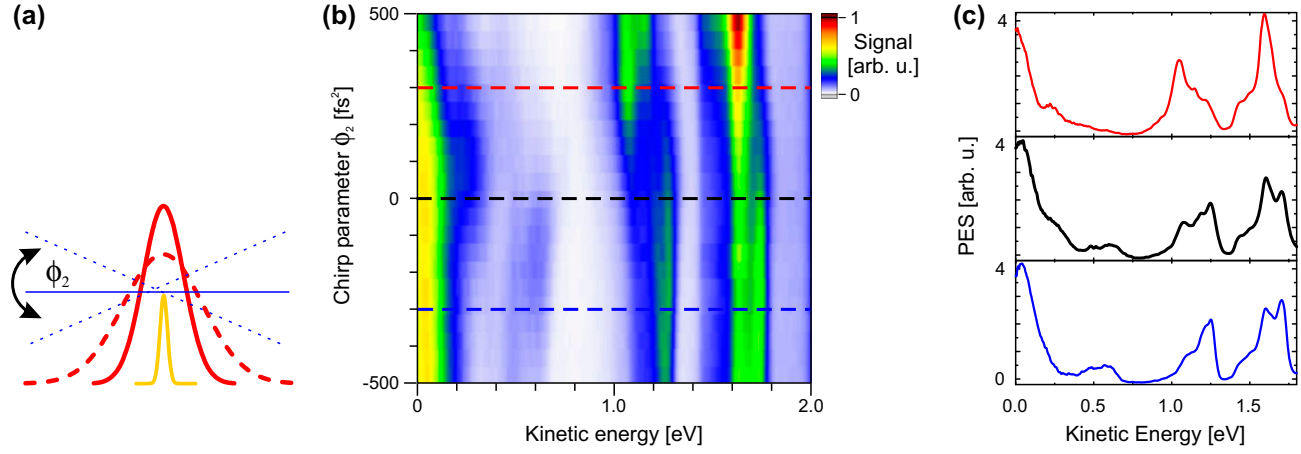

Figure 9. (a) The chirp of the IR control pulse is varied and the system is probed during the interaction with the control pulse at $\tau = 0$ fs. (a) Measured PES resulting from a chirp scan of the control pulse and probing of the system during the most intense part of the control pulse. During that time, the strongly driven atomic system is best described by the dressed states, which are mapped into the PES by ionization by both laser pulses. Consequently, all signals in the recorded spectra show the dynamics of the dressed states under chirped excitation. (c) Selected spectra from the chirp parameter scan on the left. Shown are spectra that result from interaction with a negatively chirped pulse (blue), the BWL pulse (black) and a positively chirped pulse (red).

double-peak structure of the signals (cf. black spectrum in Figure 9(c)). For chirped pulses, only one of the dressed states is populated during the interaction with the pump pulse and SPODS is realized. Accordingly, only one component of the split signals shows up in the PES for larger chirp parameters, as can be seen for the blue and the red spectra in c). Specifically, negative chirp leads to signal from the higher energetic components (blue spectrum), while positive chirp leads to signal from the lower energetic components (red spectrum). The observed signals do not directly provide new insights into the dynamics of the driven system. Still it is interesting that by tendency also the dressing of the ground state may be observed. The detected threshold photoelectrons map the SPODS signature to the continuum and thereby prove that the selective population of a distinct dressed state also holds for the ground state. However, due to the probe wavelength of $\lambda_p = 570$ nm, only electrons originating from the higher energetic component can reach the continuum. As the signal from this higher component already starts to overlap with the signal from the AT components, we did not decrease the probe wavelength. It can be extracted directly from the PES that SPODS can be observed in the signals from the ground and the excited states for the same dressed state. The population of the upper resp. lower dressed state holds for both energy levels.

Similar to the other signals present in the PES, the mixed frequency signal around 1 eV maps the transient dynamics of the system and accordingly SPODS to the photoelectron continuum.

5. Summary

In this paper, we presented a route towards a complete understanding of strong-field coherent control experiments. For our prototype studies, we chose near-resonant chirped excitation of potassium atoms which serves as a model system for resonant strong-field control. Combining a two-colour pump–probe scheme for time-resolved measurements with photoelectron spectroscopy for quantum phase-sensitive detection, we were able to simultaneously observe final state and transient excitation dynamics in the strongly driven atom. Both aspects, i.e. the bare state and the dressed state dynamics, carry vital information on the physical mechanism at play and together provide a comprehensive picture of the strong-field control process.

In a first step, we studied near-resonant Rabi cycling to calibrate the interaction strength and discriminate between weak- and strong-field excitation. Next, we examined non-perturbative chirped excitation, closely related to the well-established strong-field control scenario RAP. In a series of time-resolved and chirp-dependent experiments, we investigated the population and time evolution of the final state after the excitation, as well as the transient dressed state dynamics during the interaction with the chirped control pulse. We found that for our experimental conditions, excitation with down-chirped pulses leads to adiabatic interaction, involving the selective population of the upper dressed state throughout the interaction and a complete population transfer to the $4p_{3/2}$ state. In contrast, for excitation with up-chirped pulses of the same energy, the passage through resonance was not fully adiabatic. In this semi-adiabatic case, transitions between the dressed states enabled the excitation of a coherent superposition of states $4p_{1/2}$ and $4p_{3/2}$, i.e. a fine structure wave packet. Observation and control of the corresponding wave packet dynamics were demonstrated in extended pump–probe measurements. Chirp-dependent studies of the final populations revealed the transition from the impulsive (Rabi) to the adiabatic (RAP) excitation regime for negative chirps. By probing of the system during the interaction with the chirped pulses, the transient dressing of the system was observed.

Our results highlight the power of two-colour time-resolved photoelectron spectroscopy to shed light onto the different aspects of non-perturbative coherent control. As demonstrated on the prototype scenario RAP, the scheme enables a detailed understanding of the physical mechanisms governing the control process. In view of current challenges in strong-field control, such as attosecond control of coherent electron dynamics and the control of increasingly large molecules in femtochemical applications, the importance to access all aspects of the laser-induced excitation becomes ever more evident. Investigating laser–matter interactions from all perspectives is the key to unravel the physical mechanisms of strong-field control in more complex situations.

Disclosure statement

No potential conflict of interest was reported by the authors.

Funding

This work was supported by the Deutsche Forschungsgemeinschaft via the [SPP 1840]: QUTIF and via individual grants.

References

(1) Shapiro, M.; Brumer, P. *Quantum Control of Molecular Processes*; Wiley-VCH, Berlin, 2011.
(2) Rice, S.A.; Zhao, M. *Optical Control of Molecular Dynamics*; Wiley: New York, NY, 2000.
(3) Tannor, D. *Introduction to Quantum Mechanics: A Time-Dependent Perspective*, Palgrave Macmillan: Hampshire, 2007.
(4) Bayer, T.; Braun, H.; Sarpe, C.; Siemering, R.; von den Hoff, P.; de Vivie-Riedle, R.; Baumert, T.; Wollenhaupt, M. Charge Oscillation Controlled Molecular Excitation. *Phys. Rev. Lett.* **2013,** *110,* 123003.
(5) Braun, H.; Bayer, T.; Sarpe, C.; Siemering, R.; de Vivie-Riedle, R.; Baumert, T.; Wollenhaupt, M. Coupled Electron-Nuclear Wavepacket Dynamics in Potassium Dimers. *J. Phys. B: At. Mol. Opt. Phys.* **2014,** *47,* 124015. ISI: 000337721200016.
(6) Vitanov, N.V.; Halfmann, T.; Shore, B.W.; Bergmann, K. Laser-Induced Population Transfer by Adiabatic Passage Techniques. *Annu. Rev. Phys. Chem.* **2001,** *52,* 763–809.
(7) Loy, M.M.T. Observation of Population Inversion by Optical Adiabatic Rapid Passage. *Phys. Rev. Lett.* **1974,** *32,* 814–817.
(8) Baum, J.; Tycko, R.; Pines, A. Broadband and Adiabatic Inversion of a Two-Level System by Phase-Modulated Pulses. *Phys. Rev. A* **1985,** *32,* 3435–3447.
(9) Melinger, J.S.; Gandhi, S.R.; Hariharan, A.; Tull, J.X.; Warren, W.S. Generation of Narrowband Inversion with Broadband Laser Pulses. *Phys. Rev. Lett.* **1992,** *68,* 2000–2003. DOI:10.1103/PhysRevLett.68.2000.
(10) Broers, B.; van Linden van den Heuvell, H.B.; Noordam, L.D. Efficient Population Transfer in a Three-Level Ladder System by Frequency-Swept Ultrashort Laser Pulses. *Phys. Rev. Lett.* **1992,** *69,* 2062–2065.
(11) Cao, J.; Bardeen, C.J.; Wilson, K.R. Molecular 'π Pulses' for Total Inversion of Electronic State Population. *Phys. Rev. Lett.* **1998,** *80,* 1406–1409.
(12) Malinovsky, V.S.; Krause, J.L. Efficiency and Robustness of Coherent Population Transfer with Intense, Chirped Laser Pulses. *Phys. Rev. A* **2001,** *63,* 43415.
(13) Krug, M.; Bayer, T.; Wollenhaupt, M.; Sarpe-Tudoran, C.; Baumert, T.; Ivanov, S.S.; Vitanov, N.V. Coherent Strong-Field Control of Multiple States by a Single Chirped Femtosecond Laser Pulse. *New J. Phys.* **2009,** *11,* 105051.
(14) Schneider, J.; Wollenhaupt, M.; Winzenburg, A.; Bayer, T.; Köhler, J.; Faust, R.; Baumert, T. Efficient and Robust Strong-Field Control of Population Transfer In Sensitizer

Dyes with Designed Femtosecond Laser Pulses. *Phys. Chem. Chem. Phys.* **2011,** *13,* 8733–8746.
(15) Wollenhaupt, M.; Präkelt, A.; Sarpe-Tudoran, C.; Liese, D.; Baumert, T. Quantum Control by Selective Population of Dressed States Using Intense Chirped Femtosecond Laser Pulses. *Appl. Phys. B: Lasers Opt.* **2006,** *82,* 183–188.
(16) Bayer, T.; Wollenhaupt, M.; Braun, H.; Baumert, T. Ultrafast and Efficient Control of Coherent Electron Dynamics via SPODS. In *Advances in Chemical Physics*, Brumer, P., Rice, S.A., Dinner, A.R., Eds. Vol. 159. Wiley: Hoboken, NJ, 2016; pp 235–282.
(17) Zamith, S.; Bouchene, M.A.; Sokell, E.; Nicole, C.; Blanchet, V.; Girard, B. Pump Probe Experiment in Atomic Fine Structure Levels: Observation of the Oscillation of an Angular Wavepacket. *Eur. Phys. J. D: At. Mol. Opt. Plasma Phys.* **2000,** *12,* 255–261.
(18) Chatel, B.; Bigourd, D.; Weber, S.; Girard, B. Coherent Control of Spinorbit Precession with Shaped Laser Pulses. *J. Phys. B: At. Mol. Opt. Phys.* **2008,** *41,* 74023.
(19) Bayer, T.; Wollenhaupt, M.; Sarpe-Tudoran, C.; Baumert, T. Robust Photon Locking. *Phys. Rev. Lett.* **2009,** *102,* 023004-1–023004-4.
(20) Wollenhaupt, M.; Bayer, T.; Vitanov, N.V.; Baumert, T. Three-State Selective Population of Dressed States via Generalized Spectral Phase-Step Modulation. *Phys. Rev. A* **2010,** *81,* 053422-1–053422-9.
(21) Wollenhaupt, M.; Krug, M.; Köhler, J.; Bayer, T.; Sarpe-Tudoran, C.; Baumert, T. Photoelectron Angular Distributions from Strong-Field Coherent Electronic Excitation. *Appl. Phys. B: Lasers Opt.* **2009,** *95,* 245–259.
(22) Köhler, J.; Wollenhaupt, M.; Bayer, T.; Sarpe, C.; Baumert, T. Zeptosecond Precision Pulse Shaping. *Opt. Express* **2011,** *19,* 11638–11653.
(23) Wollenhaupt, M.; Präkelt, A.; Sarpe-Tudoran, C.; Liese, D.; Bayer, T.; Baumert, T. Femtosecond Strong-Field Quantum Control with Sinusoidally Phase-Modulated Pulses. *Phys. Rev. A* **2006,** *73,* 063409-1–063409-15.
(24) Wollenhaupt, M.; Assion, A.; Baumert, T. *Springer Handbook of Lasers and Optics.* Vol. 2. Dordrecht: Springer; 2012.
(25) Sokell, E.; Zamith, S.; Bouchene, M.A.; Girard, B. Polarization-Dependent Pump-Probe Studies in Atomic Fine-Structure Levels: Towards the Production of Spin-Polarized Electrons. *J. Phys. B: At. Mol. Opt. Phys.* **2000,** *33* (11), 2005–2015.
(26) Goulielmakis, E.; Loh, Z.H.; Wirth, A.; Santra, R.; Rohringer, N.; Yakovlev, V.S.; Zherebtsov, S.; Pfeifer, T.; Azzeer, A.M.; Kling, M.F.; Leone, S.R.; Krausz, F. Real-Time Observation of Valence Electron Motion. *Nature* **2010,** *466,* 739–743.
(27) Shivaram, N.; Tong, X.M.; Timmers, H.; Sandhu, A. Attosecond Quantum-Beat Spectroscopy in Helium. *J. Phys. B: At. Mol. Opt. Phys.* **2016,** *49,* 55601.
(28) Netz, R.; Feurer, T.; Roberts, G.; Sauerbrey, R.A. Coherent Population Dynamics of a Three-Level Atom in Spacetime. *Phys. Rev. A* **2002,** *65,* 043406-01–043406-12.
(29) Wollenhaupt, M.; Assion, A.; Bazhan, O.; Horn, C.; Liese, D.; Sarpe-Tudoran, C.; Winter, M.; Baumert, T. Control of Interferences in an Autler–Townes Doublet: Symmetry of Control Parameters. *Phys. Rev. A* **2003,** *68,* 015401-1–015401-4.
(30) Wollenhaupt, M.; Liese, D.; Präkelt, A.; Sarpe-Tudoran, C.; Baumert, T. Quantum Control by Ultrafast Dressed States Tailoring. *Chem. Phys. Lett.* **2006,** *419,* 184–190.
(31) Sleva, E.T.; Xavier, I.M. Jr; Zewail, A.H. Photon Locking. *J. Opt. Soc. Amer. B: Opt. Phys.* **1985,** *3,* 483–487.
(32) Bai, Y.S.; Yodh, A.G.; Mossberg, T.W. Selective Excitation of Dressed Atomic States by Use of Phase-Controlled Optical Fields. *Phys. Rev. Lett.* **1985,** *55,* 1277–1280.
(33) Kosloff, R.; Hammerich, A.D.; Tannor, D. Excitation without Demolition: Radiative Excitation of Ground-Surface Vibration by Impulsive Stimulated Raman Scattering with Damage Control. *Phys. Rev. Lett.* **1992,** *69,* 2172–2175.
(34) Malinovsky, V.S.; Meier, C.; Tannor, D.J. Optical Paralysis in Electronically Congested Systems: Application to Large-Amplitude Vibrational Motion of Ground State Na_2. *Chem. Phys.* **1997,** *221,* 67–76.

Appendix 1. Multi-pulse excitation

As a complementary study to the BWL and chirped excitation discussed so far, we applied the two-colour pump–probe scheme to investigate the interaction of potassium atoms with intense multi-pulse sequences. In this case, dressed state control is based on discrete temporal phase jumps rather than continuous variations of the temporal phase (*23*, *29*, *30*). The underlying strong-field control mechanism is Photon Locking (*31–34*) (PL). The multi-pulse sequences were generated by application of sinusoidal spectral phase masks of the form $\varphi(\omega) = A \cdot \sin[(\omega - \omega_0)T + \phi]$ to the LC-SLM, with $A = 0.5$ and $T = 120\,\mathrm{fs}$. The sine phase ϕ determines the relative optical phase between the individual sub-pulses and therefore represents the primary control parameter in the shaper based PL scenario. In the experiments presented in Figure A1, we measured two-colour PES as a function of ϕ varied over two optical cycles. The control pulse energy was set to 0.8μJ. In order to observe the transient dynamics as well as the final state populations, we fixed the time delay to $\tau = 1\,\mathrm{ps}$. In view of the transient excitation dynamics, the AT doublet around 0.4 eV in Figure A1(b) and (c) (measured) and (d) (simulated) indicates that for relative phases of $\phi \propto (2n+1)\pi/2$, $n \in \mathcal{Z}$, the selective population of a single dressed state is realized. In every first half cycle, the upper dressed state is populated, while the lower dressed state is populated in the second half cycle. According to the 4*s* and 4*p* signals, both cases are accompanied by the excitation of the atom to the 4*p* multiplet after the control pulse. In contrast, for relative phases of $\phi \propto n\pi$, no selectivity among the dressed states is obtained in the transient dynamics, and by the end of the control pulse, the bare state population has returned coherently to the ground state. Therefore, the final bare state populations oscillate at twice the frequency of the dressed state populations. These results exemplify the ability of the pump–probe scheme to also observe final state and transient excitation dynamics induced by pulse sequences with discrete optical phases, complementary to chirped excitation with a continuous optical phase.

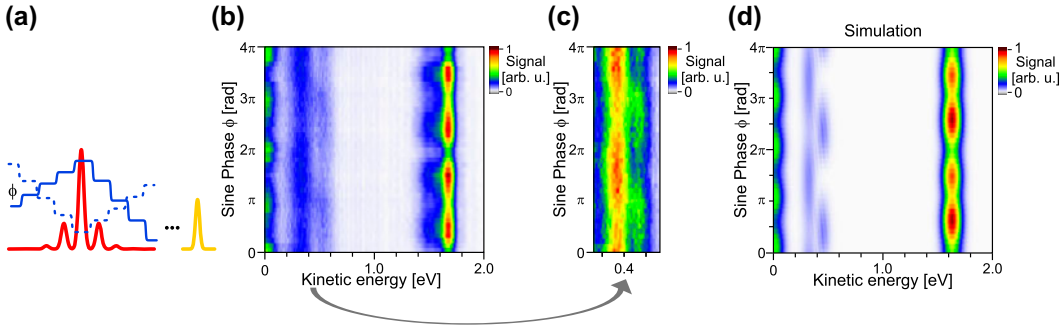

Figure A1. (a) The optical phase (blue) of the IR control pulse is varied via the phase ϕ of the sinusoidal phase mask. The delay τ between the control and the probe pulses is fixed. (b) Measured PES resulting from a phase scan of the sinusoidally phase-modulated control pulse. Again the signals generated by the probe pulse are proportional to the final populations in the atomic states while the signals created during the most intense part of the control pulse map the dynamics of the dressed states. (c) Zoom-in of the kinetic energy region of the AT doublet around 0.4 eV. (d) Simulated PES are in good agreement with the measurements.